Sea Level Variability around Japan during the Twentieth Century Simulated by a Regional Ocean Model

YOSHI N. SASAKI

Faculty of Science, Hokkaido University, Sapporo, Japan

RYOSUKE WASHIZU

School of Science, Hokkaido University, Sapporo, Japan

TAMAKI YASUDA

Japan Meteorological Agency, Tokyo, Japan

SHOSHIRO MINOBE

Faculty of Science, Hokkaido University, Sapporo, Japan

(Manuscript received 7 July 2016, in final form 23 March 2017)

ABSTRACT

Sea level variability around Japan from 1906 to 2010 is examined using a regional ocean model, along with observational data and the CMIP5 historical simulations. The regional model reproduces observed interdecadal sea level variability, for example, high sea level around 1950, low sea level in the 1970s, and sea level rise during the most recent three decades, along the Japanese coast. Sensitivity runs reveal that the high sea level around 1950 was induced by the wind stress curl changes over the North Pacific, characterized by a weakening of the Aleutian low. In contrast, the recent sea level rise is primarily caused by heat and freshwater flux forcings. That the wind-induced sea level rise along the Japanese coast around 1950 is as large as the recent sea level rise highlights the importance of natural variability in understanding regional sea level change on interdecadal time scales.

1. Introduction

Coastal sea level variability, particularly coastal sea level rise due to global warming, has attracted considerable attention because of its importance for coastal environments and management (Cazenave and Le Cozannet 2014). The global mean sea level rise from 1993 to 2012 was approximately $+3.2\,\mathrm{mm\,yr^{-1}}$ from satellite observations (Church et al. 2013). Sea level information prior to the satellite era can be obtained from tide gauge and ocean temperature (i.e., thermosteric sea level) observations (e.g., Suzuki and Ishii 2015), even though the availability of long-term data, particularly prior to the midtwentieth century, is severely limited. Global mean sea level during the twentieth century estimated from tide gauge data also exhibits a positive trend ($+1.6 \pm 0.3\,\mathrm{mm\,yr^{-1}}$; Jevrejeva et al. 2008; Church and White 2011; Ray and Douglas 2011; Hay et al. 2015). Importantly, sea level variability exhibits strong spatial dependency even on decadal and longer time scales, partly owing to wind variability (e.g., Holgate and Woodworth 2004; Sasaki et al. 2008; Merrifield et al. 2009; McGregor et al. 2012; Zhang and Church 2012). To assess coastal sea level change, it is therefore important to understand regional sea level variability on decadal and longer time scales, as well as global mean sea level rise.

Recently, the Japan Meteorological Agency (JMA) estimated the coastal sea level along Japan since 1906 by averaging sea level data at four tide gauge stations (Fig. 1) (http://www.data.jma.go.jp/gmd/kaiyou/english/sl_trend/sea_level_around_japan.html). JMA selected these stations because the sea levels of these stations do not show suspicious trends or jumps and this sea level time series is well correlated with the sea level time

Corresponding author: Yoshi N. Sasaki, sasakiyo@sci.hokudai.ac.jp

DOI: 10.1175/JCLI-D-16-0497.1

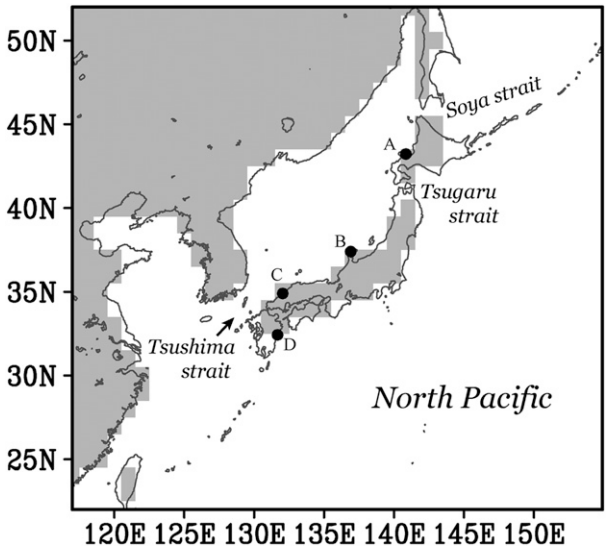

FIG. 1. Locations of the four tide gauge stations (closed circles) and the land mask of the model (light gray areas). The labels A, B, C, and D denote Oshoro (43.22°N, 140.87°E), Wajima (37.40°N, 136.90°E), Hamada (34.90°N, 132.07°E), and Hosojima (32.43°N, 131.67°E), respectively.

series averaged over 16 tide gauge stations along the Japanese coast for the data-abundant period after 1960. Interestingly, the sea level time series along the Japanese coast shows prominent interdecadal variability (the black line in Fig. 2a), in contrast to the global mean sea level, the variability of which on interdecadal time scales tends to be reduced by the global averaging. Similar large sea level fluctuations on interdecadal time scales have been reported in other regions (Dangendorf et al. 2014; Becker et al. 2014). One of the most striking features of the coastal sea level along Japan is the high sea level around 1950, which is also observed in the ocean thermosteric sea level data (the green line in Fig. 2a) (Ishii et al. 2006). The amplitude of the sea level anomaly (SLA) during this period is comparable to that in the last decade. Note that this recent high sea level is related to a positive trend starting in the 1980s. The positive trend after 1993 along the Japanese coast is $+2.7\,\mathrm{mm\,yr^{-1}}$, comparable to the aforementioned global mean sea level rise. Because the Japanese coast is one of the most densely populated areas of the world, the Organisation for Economic Cooperation and Development (OECD) report (Nicholls et al. 2008) ranked 3 cities along the Japanese coast as being in the top 20 cities in terms of assets exposed to coastal flooding in the future global warming. Therefore, clarifying the mechanisms of coastal sea level variability along Japan is highly relevant to society. Nevertheless, there are no studies investigating the mechanism of the high sea level around 1950, even though several studies have examined long-term coastal sea level changes along Japan (Senjyu et al. 1999; Yasuda and Sakurai 2006; Sasaki et al. 2014; Nakanowatari and Ohshima 2014; Liu et al. 2016). The purpose of this study is, therefore, to examine interdecadal sea level variability along the Japanese coast, particularly the high sea level around 1950 using a regional ocean model.

2. Data and methods

a. Observational sea level data

To validate our model results, we employed two observational datasets. The annual mean coastal sea level of Japan from 1906 to 2010 was obtained from the JMA website (http://www.data.jma.go.jp/gmd/kaiyou/shindan/a_1/sl_trend/sl_trend.html). This time series is the simple average of the sea level at four tide gauge stations (Fig. 1). The stations at Oshoro, Wajima, and Hosojima belong to the Geospatial Information Authority of Japan. These tide gauge data can also be obtained from the Permanent Service for Mean Sea Level or the Coastal Movements Data Center website (http://cais.gsi.go.jp/cmdc/center/annual.html; in Japanese). There are another six tide gauge stations that have a long temporal coverage along the Japanese coast, but JMA does not use them owing to suspicious sea level trends or jumps. To obtain independent information concerning the long-term sea level around Japan, we also used monthly thermosteric sea level data estimated from temperature observations (0–700 m) from 1945 to 2010 by Ishii and Kimoto (2009). Note that the analysis error (not including instrumental error) of this dataset is large in the early periods, particularly prior to 1950, owing to sparse observations.

b. Model

We employed the Regional Ocean Modeling System (ROMS), which solves free surface primitive equations with the hydrostatic and Boussinesq approximations on a generalized terrain-following sigma vertical coordinate system (Haidvogel et al. 2000; Shchepetkin and McWilliams 2005). To simulate sea level variability in the western North Pacific, the model domain covers the area from 30°S to 61°N and from 100°E to 80°W with a horizontal resolution of 1° longitude × 1° latitude and a vertical resolution of 32 sigma levels. The Tsushima, Tsugaru, and Soya Straits around Japan are open in the simulation (Fig. 1).

The model was run from 1871 to 2010 starting from a state of rest and the climatological temperature and salinity fields of the *World Ocean Atlas 2009* (Antonov et al. 2010; Locarnini et al. 2010). The daily surface wind stress (WS) was obtained from the National Oceanic and Atmospheric Administration Twentieth Century Reanalysis (20CR) data (Compo et al. 2011). The surface

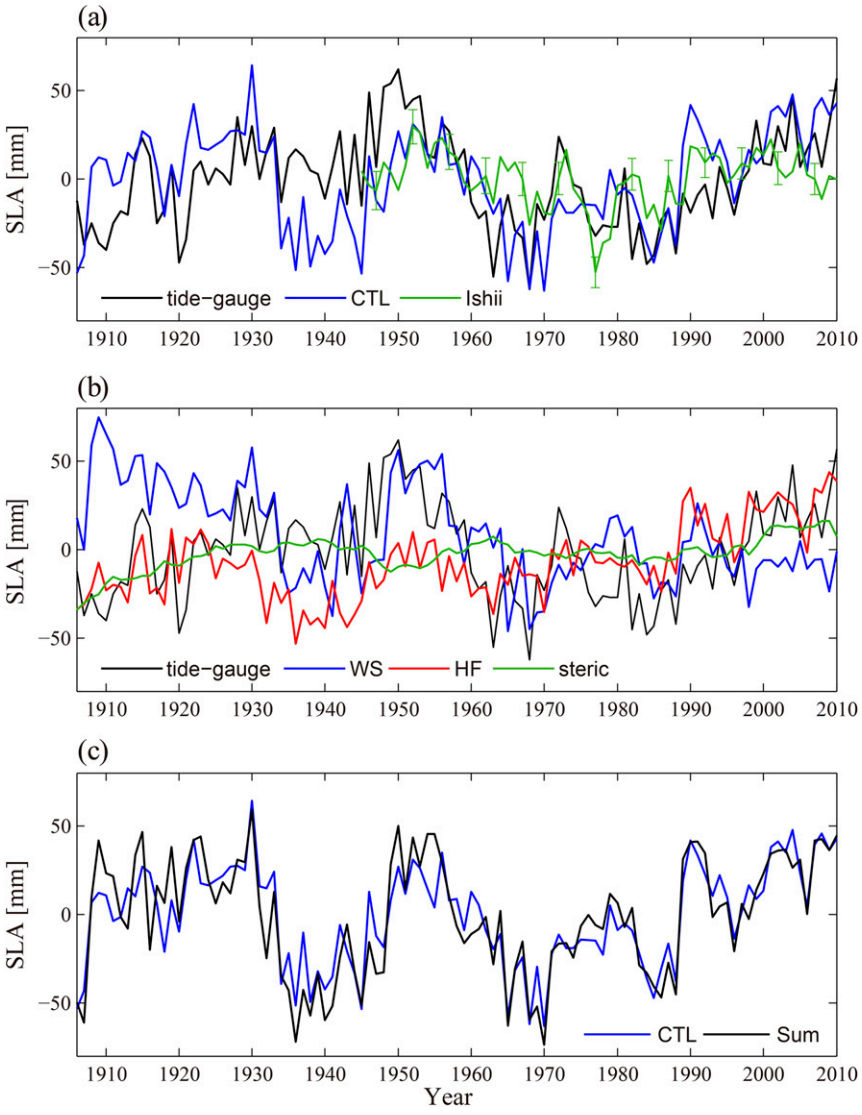

FIG. 2. (a) Annual mean SLAs along the coast of Japan in the tide gauge data (black), the CTL run (blue), and the thermosteric sea level data by Ishii and Kimoto (2009) (green). The standard deviations of the analysis error of the thermosteric sea level are shown for each 5-yr period as error bars, wherein the errors in each month are assumed to be independent. (b) Annual mean SLAs along the coast of Japan in the tide gauge data (black), the WS run (blue), the HF run (red), and the domain-averaged steric SLAs in the CTL run (green). (c) Annual mean SLAs along the coast of Japan in the CTL run (blue) and the sum of those in the WS and HF runs and the domain-averaged steric SLAs in the CTL run (black). The reference period of the SLAs is 1945–2010.

heat flux was calculated using the bulk formula by Fairall et al. (1996) from daily atmospheric variables of the 20CR data and simulated sea surface temperature. Temperature and salinity at all depths along the model's lateral boundaries and sea surface salinity were restored with a time scale of 30 days to the corresponding monthly mean values of the Simple Ocean Data Assimilation, version 2.2.4, reanalysis product (Giese and Ray 2011). Hereafter, we refer to this as the control (CTL) run. To exclude the adjustment period from the initial values and to match the period of the observation data, we analyzed the hindcast output from 1906 to 2010. Note that the results are robust if the climatology of the CTL run from 1871 to 2010 is used as the initial conditions for the temperature and salinity (not shown).

In addition to the CTL run, to clarify the mechanism of sea level variability around Japan, we conducted two sensitivity experiments. Similar approaches have been used by Piecuch and Ponte (2012, 2013), Stammer et al. (2013), and Forget and Ponte (2015). In one experiment

[the heat and freshwater flux (HF) run], the daily climatology of the surface wind stress was used, with the other model settings being the same as those of the CTL. Therefore, variability on time scales longer than the annual time scale in the model was induced via heat and freshwater fluxes through the surface and lateral boundaries, as well as via intrinsic origin (Penduff et al. 2011; Sérazin et al. 2015); note, however, that our model is not well suited for simulating intrinsic variability owing to its low horizontal resolution. In the other experiment, the atmospheric variables used to calculate the surface heat fluxes were changed to the daily climatologies, and the surface salinity, lateral temperature, and salinity fields were restored to the monthly climatologies. Because the surface wind stress varies on time scales longer than the annual time scale, we refer to this run as the WS run. Although the surface heat flux in the WS run is not a climatology due to the fluctuations induced by the simulated SST through a bulk formula, the surface heat flux in this experiment acts to damp the sea surface temperature fluctuations. Note that wind speeds to calculate the surface heat fluxes are the climatology in the WS run but are not the climatology in the HF run.

c. Methods

Since the data by Ishii and Kimoto (2009) are only available after 1945, we analyzed the annual mean SLAs relative to the 1945 to 2010 average. The coastal sea levels along Japan, both in the model and in the thermosteric sea level data by Ishii and Kimoto (2009), were defined as the average of the sea levels at the nearest grid points to the four tide gauge stations. Note that even if the coastal sea levels along Japan in the model are defined as the sea level averaged along the entire coast of Japan, the temporal variability is still essentially the same (this will be discussed in section 3a).

The water volume in the model domain is conserved owing to the Boussinesq approximation and the closed lateral boundaries (i.e., no inflow/outflow). To obtain the model domain-averaged water volume change due to steric effects, we estimated the domain-averaged steric sea level change from the simulated temperature and salinity fields (Mellor and Ezer 1995; Greatbatch 1994; Sato et al. 2006). Then, this steric sea level change was added to the sea level of the CTL run at every ocean grid point, unless otherwise stated. The steric sea level change in the domain was not added to the sea level in the WS and HF runs.

To estimate the statistical significance of the correlation coefficients, we used a Monte Carlo test. In this method, 1000 random time series were made via a phase randomization technique to create surrogate time series that have a similar spectrum of temporal variability to that of the original time series (Kaplan and Glass 1995).

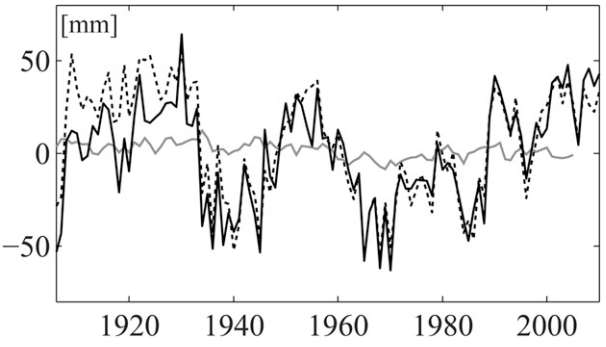

FIG. 3. Annual mean SLAs along the coast of Japan (black solid) and averaged around Japan (black dashed; 30°–46°N, 128°–146°E) in the CTL run. The multimodel ensemble mean regional SLAs (the deviation from the global mean sea level) averaged around Japan from the 37 CMIP5 models (Table 1) under the historical scenario from 1906 to 2005 are shown by gray solid line, where the sea level data in each CMIP5 model are interpolated to a 1° × 1° grid by using the bilinear interpolation before the averaging and the global mean sea level is removed from the multimodel ensemble mean sea level data.

3. Results

a. Control run

The CTL run significantly reproduces the interdecadal sea level variability along the Japanese coast. The sea level in the CTL run is high around 1950 and low around the 1970s and increases after the 1980s (the blue line in Fig. 2a). The amplitude of the simulated high sea level around 1950 is somewhat underestimated compared to the tide gauge observation (the black line in Fig. 2a); however, it is close to the thermosteric observation (the green line in Fig. 2a). The correlation coefficient of the coastal sea level time series between the tide gauge observation and the CTL run from 1906 to 2010 is 0.50 (statistically significant at the 95% confidence level). The correlation calculated after 1945 is also statistically significant at the 95% confidence level ($r = 0.63$). The performance of the model in the early periods, such as around 1940, is relatively worse, which could be due to the quality of the forcing datasets (Compo et al. 2011). The simulated sea level variation is also significantly (the 95% confidence level) correlated to the observed thermosteric sea level variation from 1945 to 2010 ($r = 0.47$). It can be noted that this simulated coastal sea level variability along Japan (the blue line in Fig. 2a) is similar to the averaged simulated sea level variability around Japan (30°–46°N, 128°–146°E; $r = 0.89$), as shown in Fig. 3. This implies that the coastal sea level variability along Japan represents the sea level variability around Japan in the model. The reason for this relation is probably because westward-propagating Rossby waves play an important role in the coastal sea level variability, as will be shown later.

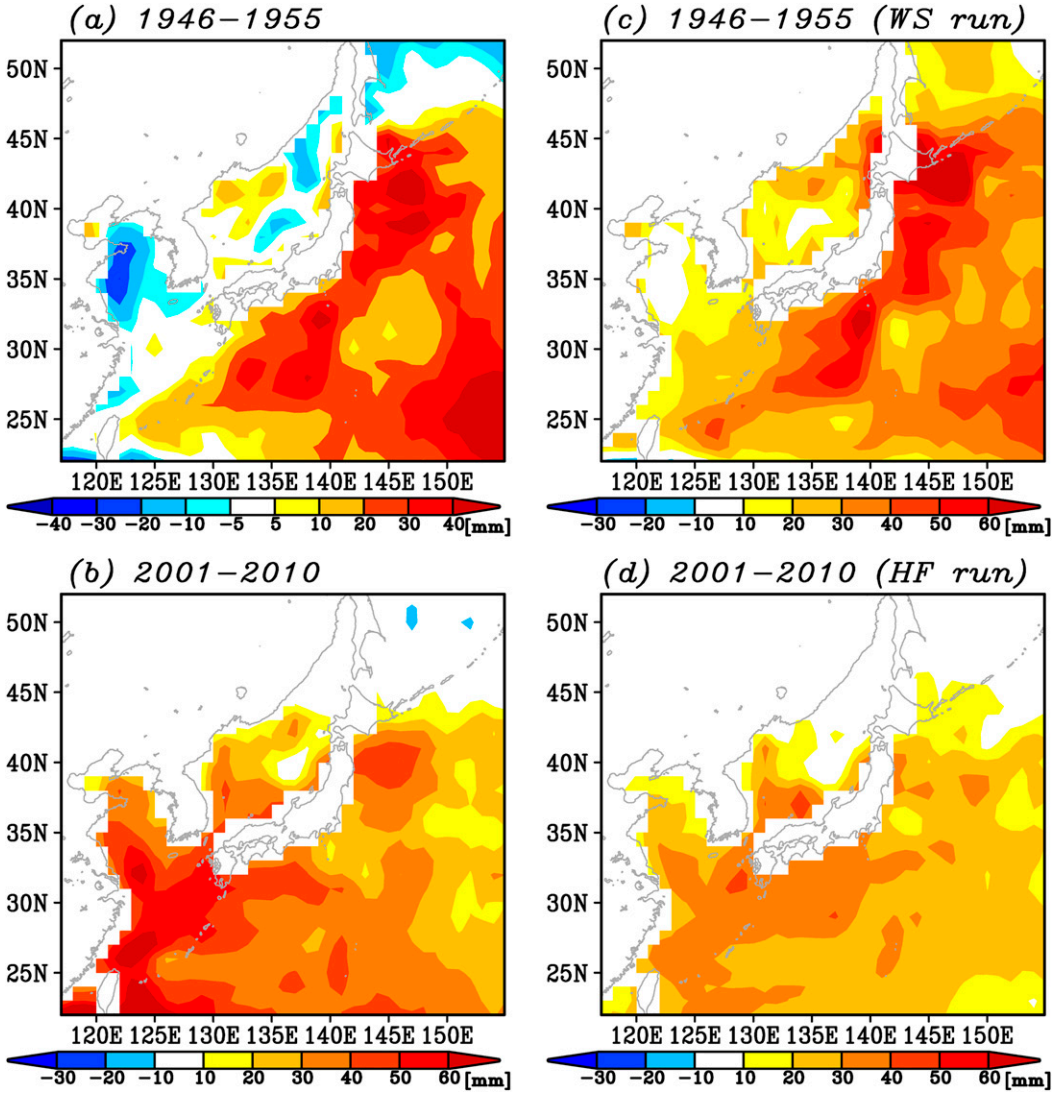

FIG. 4. SLAs averaged (a) from 1946 to 1955 and (b) from 2001 to 2010 in the CTL run, (c) from 1946 to 1955 in the WS run, and (d) from 2001 to 2010 in the HF run.

The high sea level around 1950 along the Japanese coast is associated with large-scale sea level rise in the western North Pacific (Fig. 4a). The amplitude of these SLAs over the open ocean reaches approximately 40 mm, comparable to the observed SLAs along the coast of Japan (Fig. 2a). In contrast, negative SLAs are found in the marginal seas around Japan, particularly in the East China Sea. The positive SLAs in the western North Pacific suggest that Rossby waves from the east (Qiu and Chen 2005; Sasaki et al. 2013) play an important role in the coastal sea level rise along Japan. The role of the Rossby waves will be investigated later. Conversely, the simulated SLA pattern during the most recent decade shows positive SLAs both in the western North Pacific and in the East China Sea (Fig. 4b). Therefore, the mechanism of the high sea level around 1950 is likely different from that for the most recent decade. This point will be further examined in the next subsection.

b. *Sensitivity runs*

To clarify the cause of the interdecadal sea level variability around Japan, the results of the WS and HF runs were examined. Before investigating the outputs in detail, it should be noted that the SLAs along the coast of Japan in the CTL run can be divided into three components, that is, the corresponding SLAs in the WS and HF runs (the blue and red lines in Fig. 2b, respectively) and the domain-averaged steric SLAs in the CTL run (the green line in Fig. 2b). The sum of these three components closely matches the sea level along the Japanese coast in

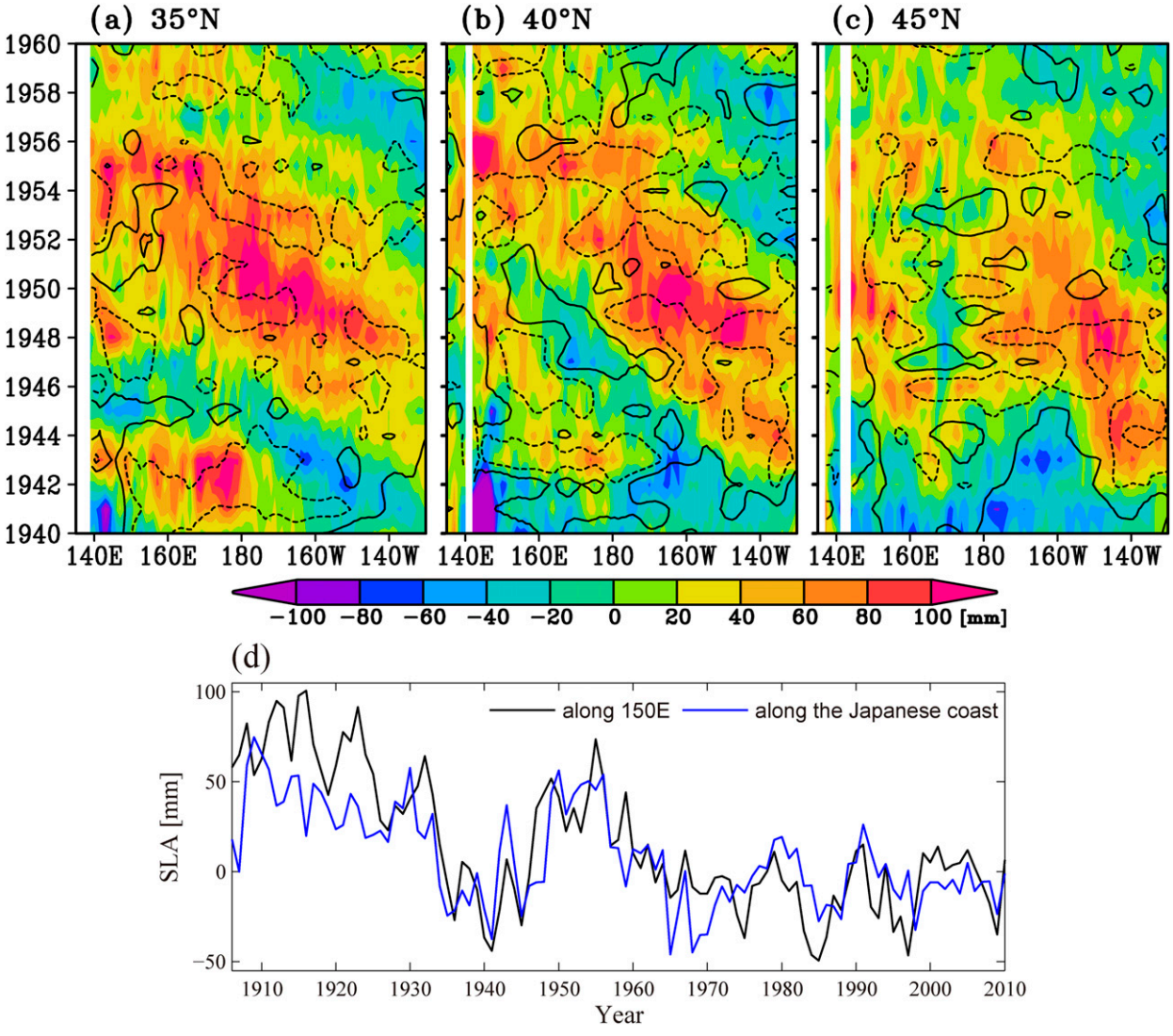

FIG. 5. Longitude–time plots of annual mean SLAs (color) along (a) 35°, (b) 40°, and (c) 45°N in the WS run. The solid (dashed) contour indicates wind stress curl anomalies of +2.5 (−2.5) × 10^{-8} N m^{-3} in (a) and (b) and of +4.0 (−4.0) × 10^{-8} N m^{-3} in (c). (d) Annual mean SLAs in the WS run along the coast of Japan (blue) and averaged between 33° and 45°N at 150°E (black).

the CTL run (Fig. 2c; $r = 0.89$). This indicates a nearly linear response of the coastal sea level along Japan to the forcings in the model, in contrast to nonlinear response in other regions (Piecuch and Ponte 2012, 2013; Forget and Ponte 2015), such as the eastern South Pacific (Piecuch and Ponte 2012), partly owing to the low horizontal resolution of the model. Therefore, we can easily separate the causes of the coastal sea level variability by investigating the results of the sensitivity runs.

Sea level variability in the WS run dominantly contributes to the high sea level around 1950 along the coast of Japan (the blue line in Fig. 2b). The SLAs of the HF run and the domain-averaged steric SLAs around 1950 are close to zero, although the HF run contributes to low sea level around 1940. Therefore, the high sea level around 1950 is primarily induced by wind stress forcing. It is worth noting that the sea level variability caused by wind stress forcing is relatively small after 1960 compared to the high sea level around 1950. This implies that the high sea level around 1950 is induced by natural variability not by anthropogenic variability, which is expected to be enhanced as time progresses. This point will be further discussed in the section 4. The spatial structure of SLAs around 1950 in the WS run (Fig. 4c) has positive anomalies in the western North Pacific and closely resembles the pattern in the CTL run (Fig. 4a), except for the small negative SLAs in the marginal seas in the WS run.

Westward-propagating signals of Rossby waves in the WS run can be seen in the longitude–time plots of SLAs along the latitude band of Japan (Figs. 5a–c). Along 35°N, the large positive SLAs emerged between 140°W and 180° in the late 1940s, and reached the east coast of Japan in the early 1950s (Fig. 5a). In addition to these signals, the positive SLAs that occurred in 1948 around 150°E and where more locally forced (Fig. 5a) likely contributed to the high sea level along the Japanese coast around 1950. Negative wind stress curl anomalies were located over both of these positive SLAs. Similar westward propagation signals of positive SLAs from west of 180° are found along 40° and 45°N (Figs. 5b,c), although their propagations are somewhat less clear. Because it takes about 4 years to propagate from 160°W to 160°E from Fig. 5a, their phase speed is about 2.9 cm s^{-1}, which is the same order of magnitude as the phase speed of the first baroclinic Rossby wave (e.g., 2.8 cm s^{-1} at 36°N; Qiu 2003). These incoming Rossby waves are expected to become coastal waves along the Japanese coast (e.g., Wu and Liu 2002). Indeed, the SLAs in the WS run averaged along 150°E, representing the integration of these incoming Rossby waves (e.g., Liu et al. 1999; Sasaki et al. 2008), show high sea level around 1950 (Fig. 5d), suggesting the importance of remote forcing. This implies that the Rossby waves from the east play a more important role than other processes, such as an alongshore wind and coastal waves propagating from the north.

To further investigate wind forcing on the SLAs, the wind stress curl change in the 20CR data around 1950 over the North Pacific is shown (Fig. 6a). During this period, negative wind stress curl anomalies were located over the northwestern, central, and northeastern North Pacific. Because negative wind stress curl anomalies cause positive SLAs via Ekman convergence and associated Rossby wave propagation (Liu et al. 1999; Vivier et al. 1999), this wind change is consistent with the sea level rise in the western North Pacific and along the Japanese coast (Fig. 4a).

Figure 6b shows the corresponding atmospheric change in the 1000-hPa geopotential height in winter. A similar pattern can be observed for the annual mean anomaly of the 1000-hPa geopotential height, except with weaker amplitude. The broad positive anomalies are located over the northern North Pacific and the Bering Sea with a peak over the Gulf of Alaska. These positive pressure anomalies are consistent with the negative wind stress curl anomalies in these locations (Fig. 6a). This atmospheric pattern indicates a weakening of the Aleutian low around 1950, which has been previously reported (e.g., Minobe 1997), suggesting a relation to the Pacific decadal oscillation (PDO) (Mantua et al. 1997).

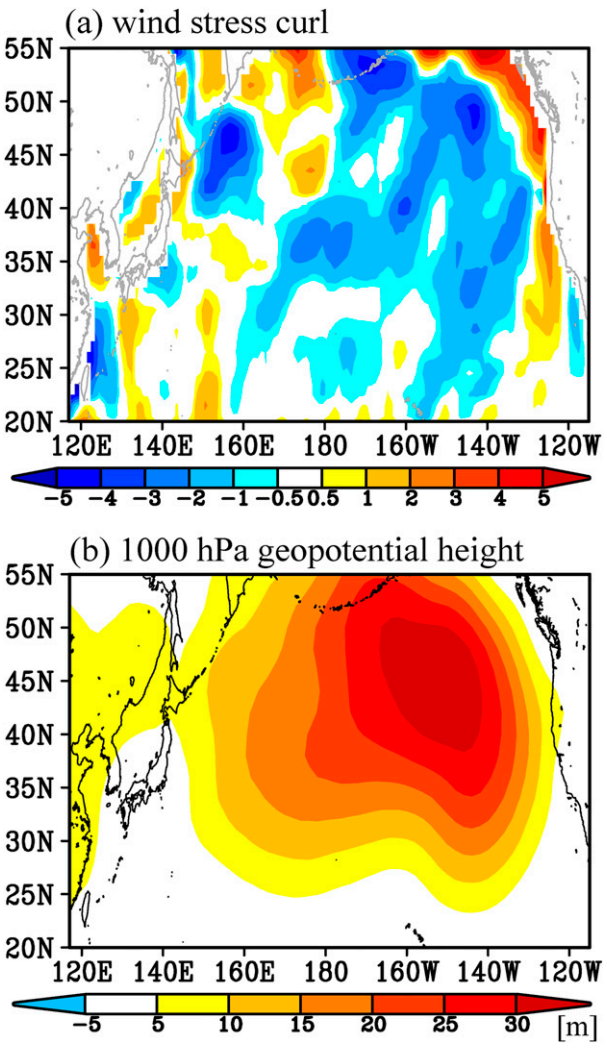

FIG. 6. (a) Annual mean wind stress curl anomalies (10^{-8} N m^{-3}) and (b) wintertime (January–March) 1000-hPa geopotential height anomalies (m) of the 20CR data averaged from 1946 to 1955.

For a further investigation of the relation between the coastal sea level variability and climate modes, we have defined climate modes by performing an EOF analysis for sea surface temperature in the CTL run (Fig. 7). Figure 7a shows that the principal component of the first EOF mode from the model is highly correlated with the observed PDO index ($r = 0.91$; http://research.jisao.washington.edu/pdo/). On the other hand, the second EOF mode is significantly related to the wintertime western Pacific pattern defined by Wallace and Gutzler (1981) ($r = 0.52$; Fig. 7b). The first and second EOF modes explain 11.4% and 6.5% of the total SST variance, respectively. Interestingly, the coastal SLAs along Japan in the WS run are correlated to the aforementioned first EOF mode ($r = -0.36$; Fig. 7c) and are lagged by 2 years for the second EOF mode ($r = -0.31$; Fig. 7d); both correlations

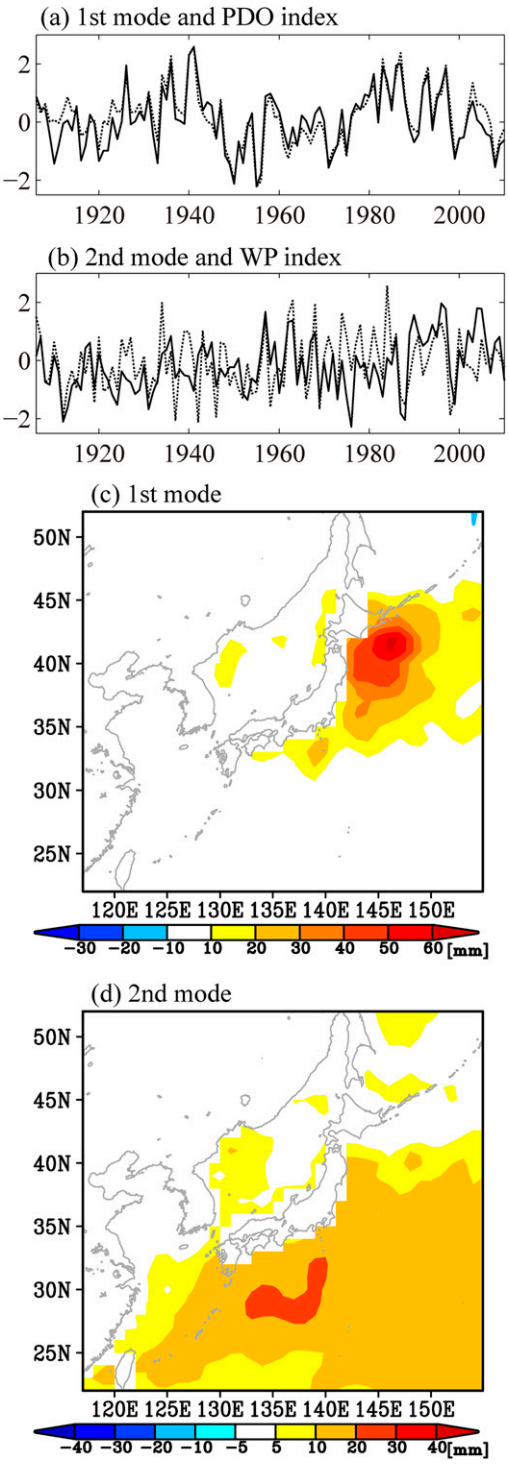

FIG. 7. (a) Principal component of the first EOF mode (PC1) of sea surface temperature in the North Pacific (20°–60°N, 120°E–120°W) in the CTL run (solid) and the observed PDO index (dashed). (b) As in (a), but for the principal component of the second EOF mode (PC2; solid) and the observed WP index (dashed). These four time series are normalized during 1945–2010. (c) Regression coefficients of SLAs in the WS run on PC1. The SLAs are shown with the sign reversed for ease of interpretation. (d) As in (c), but for PC2, where PC2 leads by 2 years. Again, the SLAs are shown with the sign reversed.

are significant at the 95% confidence level. This result suggests that the sea level variability along the Japanese coast is related to several climatic modes, consistent with Roberts et al. (2016), who showed the importance of several climate modes in sea level variability in the North Pacific. From a viewpoint of the high sea level along the Japanese coast around 1950, the principal component of the first mode shows the rapid phase change around 1950 and has negative peaks during the 1950s. The mean value of the principal component of the first mode from 1946 to 1955 is −0.88. Thus, high sea level along the Japanese coast is related to a negative phase of the PDO, consistent with the weakening of the Aleutian low (Fig. 6b).

Conversely, the mechanism for the recent sea level rise is different from that of the high sea level observed around 1950 (Fig. 2b). The linear trend of SLAs along the Japanese coast from 1993 to 2010 in the CTL run is $+2.2\,\mathrm{mm\,yr^{-1}}$, which is comparable to that of the tide gauge data ($+2.7\,\mathrm{mm\,yr^{-1}}$). For reference, the global mean sea level rise during this period from satellite observations is $+3.2\,\mathrm{mm\,yr^{-1}}$ (Church et al. 2013). The sea level rise in the CTL run is primarily attributed to the HF component and the domain-averaged steric component (the red and green lines in Fig. 2b; +1.7 and $+1.2\,\mathrm{mm\,yr^{-1}}$, respectively). The spatial pattern of the SLAs from 2001 to 2010 in the HF run (Fig. 4d) is similar to that in the CTL run (Fig. 4b). The trend in the WS run during this period is quite small ($-0.1\,\mathrm{mm\,yr^{-1}}$). Therefore, the sea level variability in the HF run and the domain-averaged steric sea level variability induced the most recent coastal sea level rise. Both SLAs are caused by heat and freshwater flux changes; however, a detailed analysis of these processes is beyond the scope of this study. It should be noted that freshwater forcing in our simulation is represented by restoring toward monthly mean salinity of the SODA dataset at the surface and lateral boundaries. Also, note that the domainwide sea level rise during the most recent three decades in the CTL run (the green line in Fig. 2b) can also be seen in the observational thermosteric sea level averaged over the same region. Indeed, the domain-averaged steric sea level change in the CTL run is consistent with the observational thermosteric sea level change averaged over the same region from 1945 to 2010 (Fig. 8; $r = 0.74$).

4. Summary and discussion

We examined the sea level variability around Japan from 1906 to 2010 using ROMS (Fig. 1). The model simulation significantly reproduces the observed interdecadal sea level variability along the Japanese coast (i.e., the high sea level around 1950, the following low sea level in the 1970s, and the sea level rise during the

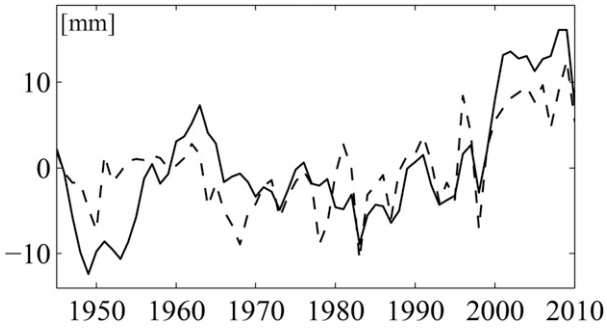

FIG. 8. The domain-averaged steric SLAs in the CTL run (solid) and in the thermosteric sea level data by Ishii and Kimoto (2009) (dashed).

most recent three decades) (Fig. 2a). The high sea level along the Japanese coast around 1950 is associated with the sea level rise in the western North Pacific (Figs. 3 and 4a). The sensitivity runs reveal that the high sea level around 1950 was induced by negative wind stress curl anomalies over the North Pacific (Figs. 2b, 5, and 6a). This wind stress change is characterized by a weakening of the Aleutian low in winter and a negative phase of the PDO (Figs. 6b and 7). In contrast, the most recent sea level rise along the Japanese coast is primarily caused by heat and freshwater forcings (Figs. 2b and 4d). Therefore, the high coastal sea level along Japan around 1950 induced by wind variability is as large as the sea level rise during the most recent three decades induced by heat and freshwater fluxes. This highlights the importance of natural variability in understanding regional sea level change even on interdecadal time scales.

To further clarify the importance of natural variability in the high sea level around 1950, we examine multimodel ensemble mean sea level data (IPCC output variable zos) from the 37 CMIP5 models under the historical scenario (Table 1; Taylor et al. 2012). The multimodel ensemble mean method reduces natural variability, which has different phases of climate modes in each coupled simulation but keeps forced sea level variability. The gray line in Fig. 3 shows the multimodel ensemble mean SLAs from 1906 to 2005 averaged around Japan (30°–46°N, 128°–146°E), where the global mean sea level is removed from the multimodel ensemble mean sea level data, since the multimodel ensemble mean global mean sea level time series does not show a peak around 1950 (e.g., Church et al. 2013). Obviously, the multimodel ensemble mean sea level variability around Japan does not show the high sea level around 1950, supporting that the high sea level was caused by natural variability.

The two peaks of the coastal sea level along Japan around 1950 and during the most recent decade could be regarded as part of a 60-yr oscillation seen in the global mean sea level and superimposed on the trend of sea level increase (e.g., Jevrejeva et al. 2008). Using tide gauge observations during the twentieth century, Chambers et al. (2012) reported that a 60-yr oscillation is prominent in the western North Pacific. Although several studies have suggested a relationship between the 60-yr oscillation of the sea level and climate modes, our study indicates that the mechanisms for these two peaks of high sea level along the Japanese coast are different (Fig. 2b). Therefore, this suggests that the 60-yr oscillation of sea level, at least in the western North Pacific, is related to several climatic modes.

One shortcoming of our simulation was its low horizontal resolution. Because of this shortcoming, the narrow and intense western boundary currents around Japan cannot be properly resolved in the model. For example, the northward (southward) shifts of the

TABLE 1. CMIP5 models used in the present study. The first ensemble of each model is analyzed.

Model	Country
ACCESS1.0	Australia
ACCESS1.3	Australia
BCC_CSM1.1(m)	China
BCC_CSM1.1	China
CanESM2	Canada
CCSM4	United States
CESM1(BGC)	United States
CESM1(WACCM)	United States
CMCC-CESM	Italy
CMCC-CM	Italy
CMCC-CMS	Italy
CNRM-CM5	France
CSIRO Mk3.6.0	Australia
EC-EARTH	European Consortium
FGOALS-g2	China
FGOALS-s2	China
FIO-ESM	China
GFDL CM3	United States
GFDL-ESM2G	United States
GFDL-ESM2M	United States
GISS-E2-R-CC	United States
GISS-E2-R	United States
HadGEM2-CC	United Kingdom
HadGEM2-ES	United Kingdom
INM-CM4.0	Russia
IPSL-CM5A-LR	France
IPSL-CM5A-MR	France
IPSL-CM5B-LR	France
MIROC5	Japan
MIROC-ESM-CHEM	Japan
MIROC-ESM	Japan
MPI-ESM-LR	Germany
MPI-ESM-MR	Germany
MRI-CGCM3	Japan
MRI-ESM1	Japan
NorESM1-ME	Norway
NorESM1-M	Norway

Kuroshio Extension jet result in high (low) sea level along the southeast coast of Japan (Sasaki et al. 2014); however, our simulation missed this regional high sea level. In addition, the straits around Japan (see Fig. 1) are wider and deeper than those in the real ocean. Therefore, coastal waves easily propagate along the coast of Japan compared to in the real ocean (Tsujino et al. 2008). These problems likely result in a weak spatial contrast of the SLAs along the coast of Japan, although our focus is sea level variability along the entire coast of Japan. Furthermore, the low horizontal resolution is not suitable for simulating oceanic intrinsic variability (e.g., Penduff et al. 2011; Sérazin et al. 2015) and nonlinear interactions between effects of wind stress and surface heat and freshwater forcings (Forget and Ponte 2015). Hence, a higher horizontal resolution is required to understand the spatial dependency of the coastal sea level variability along Japan.

Acknowledgments. We thank Dr. T. Suzuki for fruitful discussion. We also thank three anonymous reviewers for their constructive comments on the manuscript. This research was supported by the KAKENHI Grant-in-Aid for Scientific Research (B) Grant 26287110, which is funded by the Ministry of Education, Culture, Sports, Science, and Technology of Japan. The data for this study are obtained at the NOAA/OAR/ESRL PSD website (http://www.esrl.noaa.gov/psd/), the JMA website (http://www.data.jma.go.jp/gmd/kaiyou/shindan/a_1/sl_trend/sl_trend.html), and the Texas A&M University Simple Ocean Data Assimilation (SODA) website (http://sodaserver.tamu.edu/assim/SODA_2.2.4/).

REFERENCES

Antonov, J. I., D. Seidov, T. P. Boyer, R. A. Locarnini, A. V. Mishonov, H. E. Garcia, O. K. Baranova, M. M. Zweng, and D. R. Johnson, 2010: *Salinity*. Vol. 2, *World Ocean Atlas 2009*, NOAA Atlas NESDIS 69, 184 pp.

Becker, M., M. Karpytchev, and S. Lennartz-Sassinek, 2014: Long-term sea level trends: Natural or anthropogenic? *Geophys. Res. Lett.*, **41**, 5571–5580, doi:10.1002/2014GL061027.

Cazenave, A., and G. Le Cozannet, 2014: Sea level rise and its coastal impacts. *Earth's Future*, **2**, 15–34, doi:10.1002/2013EF000188.

Chambers, D. P., M. A. Merrifield, and R. S. Nerem, 2012: Is there a 60-year oscillation in global mean sea level? *Geophys. Res. Lett.*, **39**, L18607, doi:10.1029/2012GL052885.

Church, J. A., and N. J. White, 2011: Sea level rise from the late 19th to the early 21st century. *Surv. Geophys.*, **32**, 585–602, doi:10.1007/s10712-011-9119-1.

——, and Coauthors, 2013: Sea level change. *Climate Change 2013: The Physical Science Basis*, T. F. Stocker et al., Eds., Cambridge University Press, 1137–1216.

Compo, G. P., and Coauthors, 2011: The Twentieth Century Reanalysis Project. *Quart. J. Roy. Meteor. Soc.*, **137**, 1–28, doi:10.1002/qj.776.

Dangendorf, S., D. Rybski, C. Mudersbach, A. Müller, E. Kaufmann, E. Zorita, and J. Jensen, 2014: Evidence for long-term memory in sea level. *Geophys. Res. Lett.*, **41**, 5564–5571, doi:10.1002/2014GL060538.

Fairall, C. W., E. F. Bradley, D. P. Rogers, J. B. Edson, and G. S. Young, 1996: Bulk parameterization of air–sea fluxes for Tropical Ocean-Global Atmosphere Coupled-Ocean Atmosphere Response Experiment. *J. Geophys. Res.*, **101**, 3747–3764, doi:10.1029/95JC03205.

Forget, G., and R. M. Ponte, 2015: The partition of regional sea level variability. *Prog. Oceanogr.*, **137**, 173–195, doi:10.1016/j.pocean.2015.06.002.

Giese, B. S., and S. Ray, 2011: El Niño variability in Simple Ocean Data Assimilation (SODA), 1871–2008. *J. Geophys. Res.*, **116**, C02024, doi:10.1029/2010JC006695.

Greatbatch, R. J., 1994: A note on the representation of steric sea level in models that conserve volume rather than mass. *J. Geophys. Res.*, **99**, 12 767–12 771, doi:10.1029/94JC00847.

Haidvogel, D. B., H. G. Arango, K. Hedstrom, A. Beckmann, P. Malanotte-Rizzoli, and A. F. Shchepetkin, 2000: Model evaluation experiments in the North Atlantic basin: Simulations in nonlinear terrain-following coordinates. *Dyn. Atmos. Oceans*, **32**, 239–281, doi:10.1016/S0377-0265(00)00049-X.

Hay, C. C., E. Morrow, R. E. Kopp, and J. X. Mitrovica, 2015: Probabilistic reanalysis of twentieth-century sea-level rise. *Nature*, **517**, 481–484, doi:10.1038/nature14093.

Holgate, S. J., and P. L. Woodworth, 2004: Evidence for enhanced coastal sea level rise during the 1990s. *Geophys. Res. Lett.*, **31**, L07305, doi:10.1029/2004GL019626.

Ishii, M., and M. Kimoto, 2009: Reevaluation of historical ocean heat content variations with time-varying XBT and MBT depth bias corrections. *J. Oceanogr.*, **65**, 287–299, doi:10.1007/s10872-009-0027-7.

——, ——, K. Sakamoto, and S. I. Iwasaki, 2006: Steric sea level changes estimated from historical ocean subsurface temperature and salinity analyses. *J. Oceanogr.*, **62**, 155–170, doi:10.1007/s10872-006-0041-y.

Jevrejeva, S., J. C. Moore, A. Grinsted, and P. L. Woodworth, 2008: Recent global sea level acceleration started over 200 years ago? *Geophys. Res. Lett.*, **35**, L08715, doi:10.1029/2008GL033611.

Kaplan, D., and L. Glass, 1995: *Understanding Nonlinear Dynamics*. Springer, 420 pp.

Liu, Z., L. Wu, and H. Hurlburt, 1999: Rossby wave–coastal Kelvin wave interaction in the extratropics. Part II: Formation of island circulation. *J. Phys. Oceanogr.*, **29**, 2405–2418, doi:10.1175/1520-0485(1999)029<2405:RWCKWI>2.0.CO;2.

Liu, Z.-J., S. Minobe, Y. N. Sasaki, and M. Terada, 2016: Dynamical downscaling of future sea level change in the western North Pacific using ROMS. *J. Oceanogr.*, **72**, 905–922, doi:10.1007/s10872-016-0390-0.

Locarnini, R. A., A. V. Mishonov, J. I. Antonov, T. P. Boyer, H. E. Garcia, O. K. Baranova, M. M. Zweng, and D. R. Johnson, 2010: *Temperature*. Vol. 1, *World Ocean Atlas 2009*, NOAA Atlas NESDIS 68, 184 pp.

Mantua, N. J., S. R. Hare, Y. Zhang, J. M. Wallace, and R. C. Francis, 1997: A Pacific interdecadal climate oscillation with impacts on salmon production. *Bull. Amer. Meteor. Soc.*, **78**, 1069–1079, doi:10.1175/1520-0477(1997)078<1069:APICOW>2.0.CO;2.

McGregor, S., A. Sen Gupta, and M. H. England, 2012: Constraining wind stress products with sea surface height observations and implications for Pacific Ocean sea level trend attribution. *J. Climate*, **25**, 8164–8176, doi:10.1175/JCLI-D-12-00105.1.

Mellor, G. L., and T. Ezer, 1995: Sea level variations induced by heating and cooling: An evaluation of the Boussinesq approximation in ocean models. *J. Geophys. Res.*, **100**, 20 565–20 577, doi:10.1029/95JC02442.

Merrifield, M. A., S. T. Merrifield, and G. T. Mitchum, 2009: An anomalous recent acceleration of global sea level rise. *J. Climate*, **22**, 5772–5781, doi:10.1175/2009JCLI2985.1.

Minobe, S., 1997: A 50–70 year climatic oscillation over the North Pacific and North America. *Geophys. Res. Lett.*, **24**, 683–686, doi:10.1029/97GL00504.

Nakanowatari, T., and K. I. Ohshima, 2014: Coherent sea level variation in and around the Sea of Okhotsk. *Prog. Oceanogr.*, **126**, 58–70, doi:10.1016/j.pocean.2014.05.009.

Nicholls, R. J., S. Hanson, C. Herweijer, N. Patmore, S. Hallegatte, J. Corfee-Morlot, J. Chateau, and R. Muir-Wood, 2008: Ranking port cities with high exposure and vulnerability to climate extremes: Exposure estimates. Paris Organisation for Economic Cooperation and Development Working Paper 1, 62 pp.

Penduff, T., and Coauthors, 2011: Sea level expression of intrinsic and forced ocean variabilities at interannual time scales. *J. Climate*, **24**, 5652–5670, doi:10.1175/JCLI-D-11-00077.1.

Piecuch, C. G., and R. M. Ponte, 2012: Buoyancy-driven interannual sea level changes in the southeast tropical Pacific. *Geophys. Res. Lett.*, **39**, L05607, doi:10.1029/2012GL051130.

——, and ——, 2013: Buoyancy-driven interannual sea level changes in the tropical South Atlantic. *J. Phys. Oceanogr.*, **43**, 533–547, doi:10.1175/JPO-D-12-093.1.

Qiu, B., 2003: Kuroshio Extension variability and forcing of the Pacific decadal oscillations: Responses and potential feedback. *J. Phys. Oceanogr.*, **33**, 2465–2482, doi:10.1175/2459.1.

——, and S. Chen, 2005: Variability of the Kuroshio Extension jet, recirculation gyre, and mesoscale eddies on decadal time scales. *J. Phys. Oceanogr.*, **35**, 2090–2103, doi:10.1175/JPO2807.1.

Ray, R. D., and B. C. Douglas, 2011: Experiments in reconstructing twentieth-century sea levels. *Prog. Oceanogr.*, **91**, 496–515, doi:10.1016/j.pocean.2011.07.021.

Roberts, C., D. Calvert, N. Dunstone, L. Hermanson, M. Palmer, and D. Smith, 2016: On the drivers and predictability of seasonal-to-interannual variations in regional sea level. *J. Climate*, **29**, 7565–7585, doi:10.1175/JCLI-D-15-0886.1.

Sasaki, Y. N., S. Minobe, N. Schneider, T. Kagimoto, M. Nonaka, and H. Sasaki, 2008: Decadal sea level variability in the South Pacific in a global eddy-resolving ocean model hindcast. *J. Phys. Oceanogr.*, **38**, 1731–1747, doi:10.1175/2007JPO3915.1.

——, ——, and ——, 2013: Decadal response of the Kuroshio Extension jet to Rossby waves: Observation and thin-jet theory. *J. Phys. Oceanogr.*, **43**, 442–456, doi:10.1175/JPO-D-12-096.1.

——, ——, and Y. Miura, 2014: Decadal sea-level variability along the coast of Japan in response to ocean circulation changes. *J. Geophys. Res.*, **119**, 266–275, doi:10.1002/2013JC009327.

Sato, Y., S. Yukimoto, H. Tsujino, H. Ishizaki, and A. Noda, 2006: Response of North Pacific ocean circulation in a Kuroshio-resolving ocean model to an Arctic Oscillation (AO)-like change in Northern Hemisphere atmospheric circulation due to greenhouse-gas forcing. *J. Meteor. Soc. Japan*, **84**, 295–309, doi:10.2151/jmsj.84.295.

Senjyu, T., M. Matsuyama, and N. Matsubara, 1999: Interannual and decadal sea-level variations along the Japanese coast. *J. Oceanogr.*, **55**, 619–633, doi:10.1023/A:1007844903204.

Sérazin, G., T. Penduff, S. Grégorio, B. Barnier, J.-M. Molines, and L. Terray, 2015: Intrinsic variability of sea level from global ocean simulations: Spatiotemporal scales. *J. Climate*, **28**, 4279–4292, doi:10.1175/JCLI-D-14-00554.1.

Shchepetkin, A. F., and J. C. McWilliams, 2005: The Regional Oceanic Modeling System (ROMS): A split-explicit, free-surface, topography-following-coordinate oceanic model. *Ocean Modell.*, **9**, 347–404, doi:10.1016/j.ocemod.2004.08.002.

Stammer, D., A. Cazenave, R. M. Ponte, and M. E. Tamisiea, 2013: Causes for contemporary regional sea level changes. *Annu. Rev. Mar. Sci.*, **5**, 21–46.

Suzuki, T., and M. Ishii, 2015: Interdecadal baroclinic sea level changes in the North Pacific based on historical ocean hydrographic observations. *J. Climate*, **28**, 4585–4594, doi:10.1175/JCLI-D-13-00103.1.

Taylor, K. E., R. J. Stouffer, and G. A. Meehl, 2012: An overview of CMIP5 and the experiment design. *Bull. Amer. Meteor. Soc.*, **93**, 485–498, doi:10.1175/BAMS-D-11-00094.1.

Tsujino, H., H. Nakano, and T. Motoi, 2008: Mechanism of currents through the straits of the Japan Sea: Mean state and seasonal variation. *J. Oceanogr.*, **64**, 141–161, doi:10.1007/s10872-008-0011-7.

Vivier, F., K. A. Kelly, and L. Thompson, 1999: Contributions of wind forcing, waves, and surface heating to sea surface height observations in the Pacific Ocean. *J. Geophys. Res.*, **104**, 20 767–20 788, doi:10.1029/1999JC900096.

Wallace, J. M., and D. S. Gutzler, 1981: Teleconnections in the geopotential height field during the Northern Hemisphere winter. *Mon. Wea. Rev.*, **109**, 784–812, doi:10.1175/1520-0493(1981)109<0784:TITGHF>2.0.CO;2.

Wu, L. X., and Z. Y. Liu, 2002: Dynamical control of Pacific Oceanic low-frequency variability on western boundary and marginal seas. *Geophys. Astrophys. Fluid Dyn.*, **96**, 201–222, doi:10.1080/03091920290020968.

Yasuda, T., and K. Sakurai, 2006: Interdecadal variability of the sea surface height around Japan. *Geophys. Res. Lett.*, **33**, L01605, doi:10.1029/2005GL024920.

Zhang, X. B., and J. A. Church, 2012: Sea level trends, interannual and decadal variability in the Pacific Ocean. *Geophys. Res. Lett.*, **39**, L21701, doi:10.1029/2012GL053240.